Volume 9
Number 31
21 August 2021
Pages 6095–6272

Journal of Materials Chemistry B

Materials for biology and medicine

rsc.li/materials-b

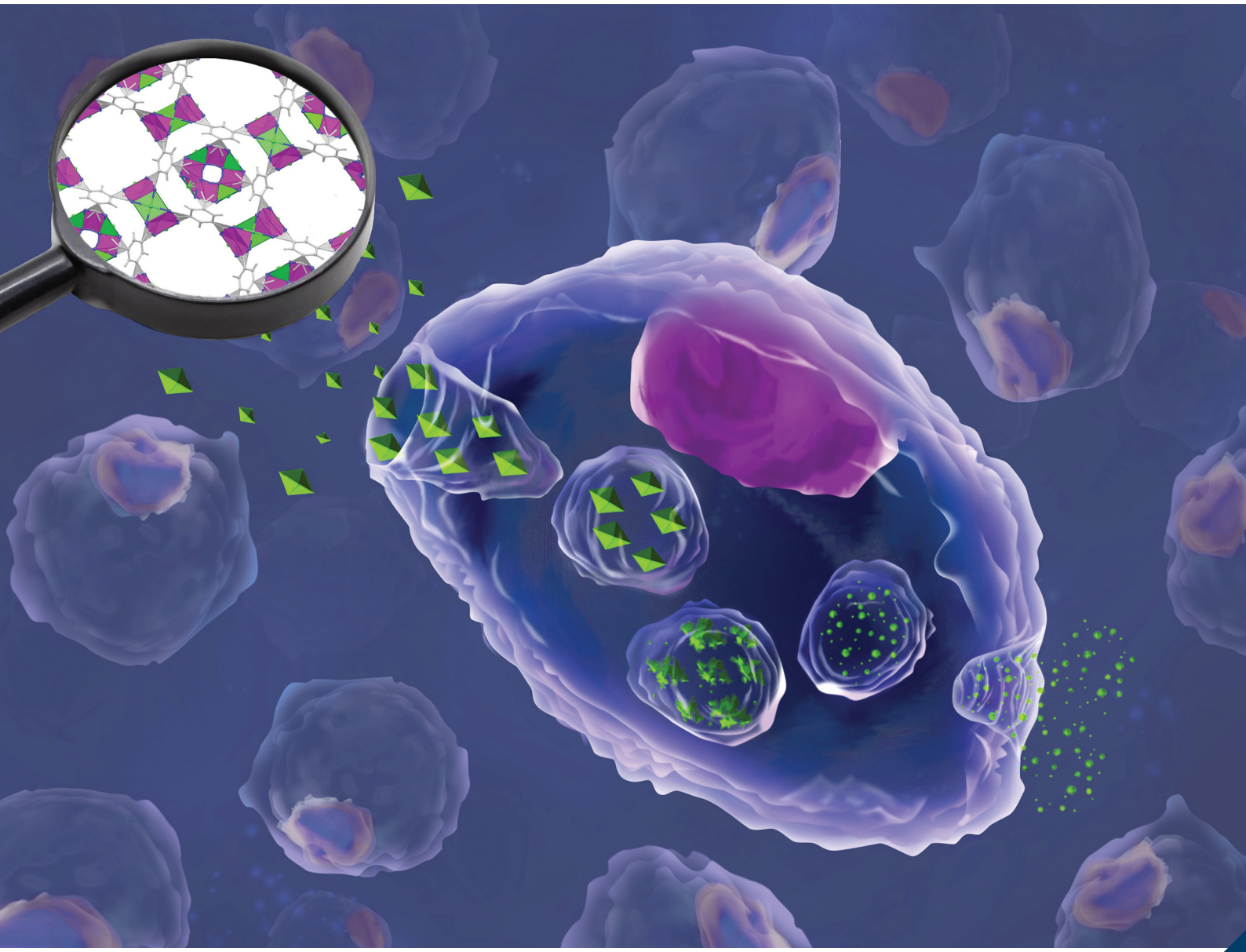

ISSN 2050-750X

ROYAL SOCIETY OF CHEMISTRY

COMMUNICATION

Isabel Abánades Lázaro, Victoria del Pozo *et al.*
The excellent biocompatibility and negligible immune response of the titanium heterometallic MOF MUV-10

Indexed in Medline!

Journal of Materials Chemistry B

ROYAL SOCIETY OF CHEMISTRY

COMMUNICATION

View Article Online
View Journal | View Issue

Open Access Article. Published on 16 July 2021. Downloaded on 4/8/2026 9:22:24 PM.
This article is licensed under a Creative Commons Attribution-NonCommercial 3.0 Unported Licence.

Check for updates

Cite this: J. Mater. Chem. B, 2021, 9, 6144

Received 30th April 2021,
Accepted 24th June 2021

DOI: 10.1039/d1tb00981h

rsc.li/materials-b

The excellent biocompatibility and negligible immune response of the titanium heterometallic MOF MUV-10†

Isabel Abánades Lázaro,*[a] Jose M. Rodrigo-Muñoz,[b] Beatriz Sastre,[b] María Romero Ángel,[a] Carlos Martí-Gastaldo[a] and Victoria del Pozo*[b]

The Ti–Ca heterometallic MOF MUV-10 exhibits good dispersibility in phosphate buffer and low phosphate-induced degradation in comparison to other MOF systems. It induces no cytotoxicity towards cells of the immune system and no inmune response, making it an attractive candidate for biomedical applications and demonstrating its safe use for other applications.

Metal–organic frameworks – porous hybrid structures composed of metal clusters linked by multitopic organic ligands[1,2] – have garnered a tremendous amount of interest over the past 20 years due to their intrinsic properties such as high porosity and unlimited chemical and structural diversity, which have made them attractive for a variety of applications related to porous and/or functional materials, including drug delivery, antibacterial coatings, gas storage and separation, water pollutant removal, magnetism, heterogeneous catalysis and photocatalysis among others. The variety of choice of metal and linker allows the design of biocompatible MOFs, which together with their tunable size, high loading capacity, easy surface modification and structural stability has positioned them as attractive alternatives for nanoscale and transdermal drug delivery systems (DDSs).

The first use of iron-based MOFs for healthcare applications was reported in 2006,[3] and since then a tremendous amount of work has been developed towards their bioapplication.[4–7] Due to their biocompatibility, iron-based MOFs are probably the most widely explored MOF materials to date. Zirconium MOFs have recently acquired attention as DDSs[6] as Zr is also biocompatible and its hard Lewis acid–base coordination characteristics generally result in higher chemical stability than iron-based MOFs, making them more amenable to surface modification[8] and resulting in higher physiological stability, a must for drug delivery applications.[6]

Titanium-based MOFs – which are photoactive and often have superior structural and chemical stability compared to other MOFs[9,10] such as Zr and Fe-based MOFs – are emerging in the literature.[11,12] Titanium has low cytotoxicity (better than any other transition metal ion apart from Fe),[5] and it is abundant. However, examples of Ti-based MOFs as DDSs are surprisingly scarce in the literature,[13–16] and despite their widely explored photocatalytic applications,[11,12] which offer the possibility for use in photodynamic therapy,[15,16] reports of their biocompatibility are difficult to find.

Assessing the biocompatibility of MOFs and the immune response towards them is imperative not only for their bioapplication, but also for any safe industrial application that involves contact with living beings or the environment. For example, MOFs could not be safely used for water treatment or surface coatings if they were not biocompatible or if they generated an immune response. However, reports of biocompatibility or immune response in studies not related to biomedical applications are uncommon.

Herein, we report the remarkable biocompatibility and negligible immune response of Ti MUV-10 heterometallic MOFs of different sizes (1700 to 28 nm), demonstrating their safe industrial application and high potential as a DDSs.

MUV-10, represented in Fig. 1a, is a highly-stable heterometallic Ti(IV)-MOF built from the assembly of tetranuclear $Ti^{IV}_2Ca^{II}_2(\mu_3\text{-}O)_2(H_2O)_4(RCO_2)_8$ clusters connected to eight neighbouring clusters by eight benzene tricarboxylate (BTC) linkers forming a cubic structure with the unit formula $[Ti_3Ca_3(\mu_3\text{-}O)_3(\mu_2\text{-}C_6H_3(CO_2)_3)_4(OH_2)_6]$.[17] This microporous framework, with a surface area close to 1000 $m^2\ g^{-1}$ and a micropore size of *ca.* 1 nm,[18] is amenable to defect engineering through the introduction of modulators, which also results in a decrease in particle size to the nanometre range due to modulator capping[19] and allows simple functionalisation. Additionally, the attachment of modulators as defect-compensating

[a] Instituto de Ciencia Molecular (ICMol), Universitat de València, Catedrático José Beltrán Martínez no. 2, Paterna 46980, Valencia, Spain. E-mail: Isabel.abanades@uv.es
[b] Department of Immunology, Instituto de Investigación Sanitaria Fundación Jiménez Díaz, Universidad Autónoma de Madrid (IIS-FJD, UAM), and CIBER de Enfermedades Respiratorias (CIBERES), Madrid 28029, Spain. E-mail: VPozo@fjd.es

† Electronic supplementary information (ESI) available: MOF synthesis, analysis and *in vitro* studies. See DOI: 10.1039/d1tb00981h

This journal is © The Royal Society of Chemistry 2021

Open Access Article. Published on 16 July 2021. Downloaded on 4/8/2026 9:22:24 PM.
This article is licensed under a Creative Commons Attribution-NonCommercial 3.0 Unported Licence.

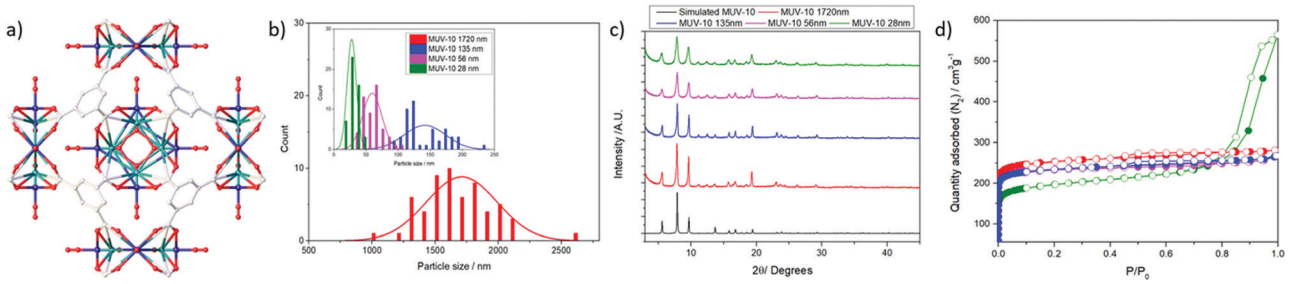

Fig. 1 (a) MUV-10 structure. Characterisation of MUV-10 MOFs with various particle sizes: (b) histograms of particle size distribution obtained using SEM with a bin size of 5 nm for the smaller samples and 150 nm for MUV-10 1720 nm; (c) PXRD patterns; (d) N_2 adsorption/desorption isotherms.

ligands indicates that defect drug loading protocols could be applied to the MUV-10 family.[20–22]

To study how MOF size affects the biocompatibility, internalisation and reactive oxygen species (ROS) production of J744 macrophages and peripheral blood mononuclear cells (PBMCs) isolated from the blood of human donors, as well as the effect on complement cascade activation that is indicative of an immune response,[23] we synthesised a series of MUV-10 MOFs of different sizes (1700, 135, 56 and 28 nm) (Fig. 1b) by tuning the linker : metal ratio and the reaction mixture pH through modulation using acetic or hydrochloric acid (see ESI† Section S.2 for detailed synthetic conditions).

All the MOFs synthesized were highly crystalline and phase pure fine powders (see ESI† Section S.4 for detailed characterization information), as shown in their PXRD profiles (Fig. 1c); their reflection signals broadened with decreasing particle size, which was determined using scanning electron microscopy (SEM). Full characterisation (ESI,† Section S.4) – including FT-IR spectroscopy, thermogravimetric analysis (TGA) and N_2 adsorption/desorption isotherms – confirmed the samples were thermally stable (Fig. S6, ESI†) and porous (Fig. 1d). Gravimetric analysis of the thermal decomposition profiles showed the samples were defective (see ESI† Section S.4)[24] with *ca.* 5–8 mol% missing linkers for samples synthesized using an excess of linker (1720, 56 and 28 nm), whereas the sample synthesised using a depleted amount of linker (136 nm) had significantly higher defect promotion, with ~25 mol% missing linkers. The BET surface areas ranged from *ca.* 1000 to *ca.* 750 $m^2\ g^{-1}$, with the decrease being related to a reduction of the particle size to *ca.* 28 nm.[25] This was also observed in the increase of external surface area and mesopore percent. The total pore volumes (P/P_0 0.9) ranged from 0.40 to 0.50 $cm^3\ g^{-1}$, with the smallest sample displaying hysteresis loops characteristic of inter-particle spacing (total pore volume at P/P_0 1 = 0.65 $cm^3\ g^{-1}$). The appearance of slightly bigger pores compared to the pristine MOF is possibly a consequence of their defective nature (Fig. S8 and S9, ESI†).

Dynamic light scattering (DLS) measurements were performed in phosphate buffered saline (PBS) 10×, where MOFs are known to suffer higher aggregation than that in water.[6] The MOFs were well-dispersed in PBS 10× without a protein spike and displayed hydrodynamic diameters close to the particle sizes determined using SEM, with the smaller samples (56 and 28 nm) displaying minor aggregation and hydrodynamic diameters twice the particle size (Fig. 2a and Fig. S11–S14, ESI†). Good colloidal dispersion is intrinsic for drug delivery applications, but this is often not the case for MOFs and surface coatings are employed to overcome this drawback.[6] MOFs are known to form a protein corona under physiological conditions (*i.e.* cell culture media and blood current) that prevents them from aggregating[26] and spiking PBS with bovine serum albumin has been shown to result in drastic improvements in their colloidal dispersion,[27] which indicates that MUV-10 may not suffer significant aggregation in cell culture media despite having unmodified surfaces.

The stability of the samples in PBS 10× (pH = 7.4) was investigated using UV–vis spectroscopic determination of linker release (benzene tricarboxylate) for the largest (1700 nm) and smallest samples (28 nm). A small burst of degradation was observed for the largest particle size (~13%) after 15 minutes, with similar release rates over the first hour to one day (*ca.* 20%) and a slightly faster release rate for the smaller sample, which degraded significantly after 7 days (~90% for the smallest and 65% for the largest sample, respectively) (Fig. 2b). However, their degradation under these simulated physiological conditions is remarkably slower than for other MOF systems currently being investigated as DDSs, such as UiO-66 (Zr)[6] and MIL-101 (Fe),[28] which release ~80% of their linkers after a few hours and Zr-fumarate MOFs with a ~60% linker release after 8 hours under comparable degradation conditions.[29] The degradation kinetics are comparable with MIL-100 (Fe), which releases *ca.* 58% of its linker after 7days, although its phosphate-induced degradation was performed using phosphate solutions 10 times less concentrated than in our experiments.[30] These results are of higher importance if we

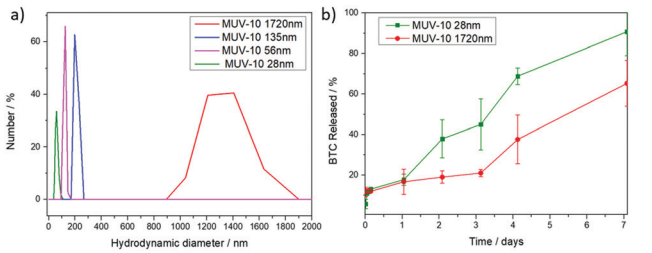

Fig. 2 (a) Dynamic light scattering measurements. (b) Phosphate-induced degradation profiles.

Open Access Article. Published on 16 July 2021. Downloaded on 4/8/2026 9:22:24 PM.
This article is licensed under a Creative Commons Attribution-NonCommercial 3.0 Unported Licence.

consider that our degradation experiments are performed without a dialysis bag, which prolongs the release profiles by adding the molecule dialysis time. This is in agreement with the increased bonding strength between metal ions and ligands, where a smaller ratio of Ti^{4+} ions results in stronger metal–O bonds than that in analogous Zr^{4+} MOFs.[10]

These results also indicate that MOFs composed of tridentate ligands might have low phosphate-induced degradation compared to those composed of bidentate ligands, given that more metal–carboxylate bonds have to be displaced.

To monitor the effect of MUV-10 particle size on its internalisation by cells of the immune system, we postsynthetically loaded the MOFs with calcein, a carboxylate-containing fluorescent molecule that cannot efficiently cross the cell membrane due to its hydrophilicity,[31] and so it is an excellent probe for the cellular internalisation of MOFs.[32] Calcein was loaded in high amounts from *ca.* 9.5 to 33.7 w/w%, the loading increased with reducing particle size, which is possibly due to the greater external surface : bulk ratio. Characterisation results (see ESI† Section S.5) suggest that calcein is attached to the metal clusters through its carboxylate units, which is in agreement with reports of calcein-loaded Zr-based MOFs.[6,32] These results show that MUV-10 is an excellent candidate for the loading of drugs or biomolecules. Using calcein as a model drug, we measured its release in PBS 10×, which showed that MUV-10 is a good drug delivery system, releasing the full amount of loaded calcein after 2 days, with a small burst release of *ca.* 30% during the first hour despite not using a dialysis bag. MUV-10 of 28 nm released *ca.* 40% after one day of exposure whereas MUV-10 of 1720 nm released *ca.* 75% of its loaded calcein (Fig. S36, ESI†), while many bare MOFs previously reported release their full cargo after a few hours in PBS.[5,6]

Fluorescence assisted cell sorting (FACS) was used to monitor the cellular internalisation of the calcein@MOFs by cells of the immune system, such as macrophages and PBMCs (see ESI† Section S.3 for detailed *in vitro* protocols). A drastic increase in their cytoplasmic fluorescence was observed after incubation with 250 μg mL^{-1} of calcein@MOFs over two hours in comparison to free calcein, with cellular internalisation being higher for PBMCs (see ESI† Section S.6). Given the different calcein loadings of the samples, as represented in Fig. 3a, the mean fluorescence intensity was normalised by the maximum amount of calcein delivered by each sample to determine which particle size demonstrated the highest internalisation (Fig. 3b). Our results indicate that the largest particle sizes were highly internalised both by J744 macrophages and PBM cells, whereas the smallest particles (56 and 28 nm) were significantly less internalised. This is of great importance if we take into account that several reports show opposite trends for the internalisation by cancer cells,[29] indicating that smaller particle sizes more easily escape uptake by cells of the immune system while enhancing their internalisation by cancer cells. This is because cells of the immune system typically internalise particles through phagocytosis and recognise more significantly particles of larger sizes, while cancer cells internalise particles through endocytosis, where membrane permeation plays an important role and hence smaller particles are internalised in a more efficient manner.[33] Importantly, the MOFs are able to deliver calcein with a more than *ca.* 20-fold increase to macrophage and PBM cells. Once proven that the MOFs are internalised by cells of the immune system, we assessed the effect on their proliferation using the MTT assay. J744 macrophages and PBMCs were incubated with the MOFs for 24 and 72 hours (see ESI† Section S.3 for protocols and S.7 for tabulated results of independent experiments). The results show excellent biocompatibility, with a cell proliferation of over 100% in all cases, even upon incubation with high concentrations of MOFs (up to 500 μg mL^{-1}), whereas incubation with 500 μg mL^{-1} of free BTC results in a decrease in J744 macrophage and PBM cell viability to *ca.* 80% after 72 hours (Fig. 3c).

The reactive oxygen species (ROS) production was studied to assess if MUV-10 induces oxidative stress in macrophages (Fig. 4a). The cells were incubated with 250 μg mL^{-1} of the different MOFs for 2 hours. The 156 nm MOF induced mild generation of ROS (*ca.* 150%) in J744 cells whereas all the other MOFs did not induce any ROS generation, which is in contrast with literature reports showing up to 200% ROS production upon incubation with similar concentrations of UiO-66 (Zr).[21] The ROS production of the 156 nm MOF could be attributed to

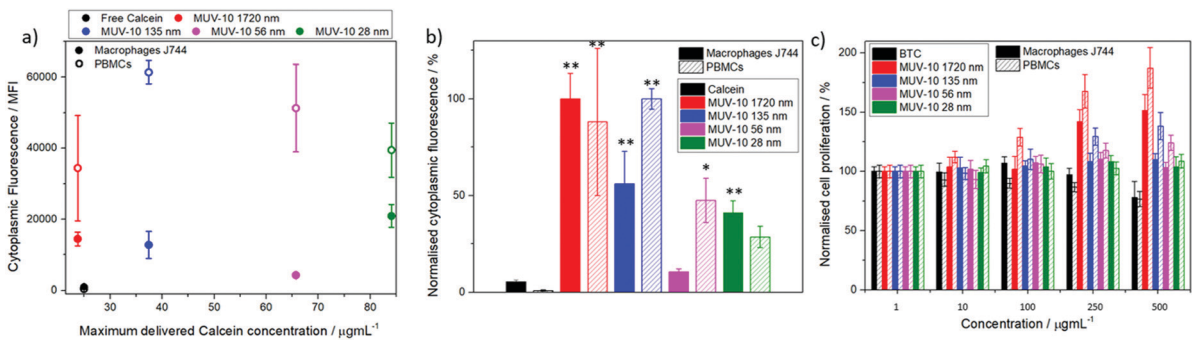

Fig. 3 Cell internalisation (a) as a function of the maximum amount of calcein delivered by each MOF based on its calcein-loading (note that free calcein for PBMCs and J744 overlaps) and (b) normalised using the calcein loading of each sample and towards the sample exhibiting the maximum fluorescence/calcein loading ratio with $^{**}p < 0.01$ and $^{*}p < 0.5$ for a one-way ANOVA against free calcein. (c) Cytotoxicity of the MUV-10 samples measured using an MTT assay towards J774 macrophage cells and human peripheral blood mononuclear cells isolated from human donors.

 This journal is © The Royal Society of Chemistry 2021

Open Access Article. Published on 16 July 2021. Downloaded on 4/8/2026 9:22:24 PM.
This article is licensed under a Creative Commons Attribution-NonCommercial 3.0 Unported Licence.

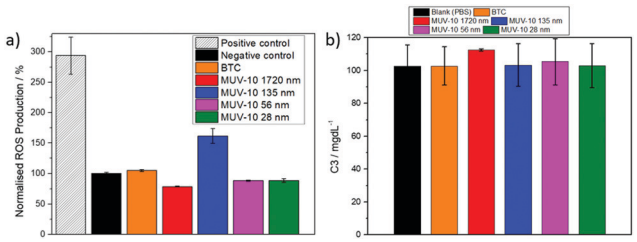

Fig. 4 Immune response following incubation with 250 μg mL^{-1} of MUV-10. (a) Reactive oxygen species generation in macrophage cells, normalisation using the untreated control (negative). (b) Complement cascade activation of the C3 complement component averaged following incubation with plasma from five different donors. A normal concentration for the C3 complement is 90–180 mg mL^{-1}.

its higher defectivity (*ca.* 23.5% missing linkers) compared to the other MOFs (*ca.* 5–8% missing linkers), which often lowers the energy of the unoccupied *d* orbitals and increases the likelihood of charge transfer.[34]

The activation of the complement cascade (C3 and C4)–a part of the immune system that eliminates foreign pathogens, often resulting in activation of phagocytic cells and inflammation[23]–was investigated following the incubating of blood plasma from five different human donors with the MOFs. Fig. 4b shows the averaged data for the C3 concentrations of the five donors after incubation with 250 μg mL^{-1} of the MOFs (see S.7, ESI† for the C4 complement), together with a control in which the blood plasma was incubated with a PBS solution (see S.7, ESI† for the C3 and C4 values of each individual donor) that showed no complement cascade activation upon treatment with each of the MOFs.

Taken together, the improved physiological stability towards phosphate-induced degradation, dispersion in PBS and immune system compatibility compared to iron- and zirconium-based MOFs suggests that MUV-10 is an excellent candidate for further investigation as a drug delivery device, with fine control over particle size and functionality made possible through the introduction of modulators. Additionally, this study demonstrates the safe use of MUV-10 for other applications given its excellent biocompatibility.

Conflicts of interest

There are no conflicts to declare.

Acknowledgements

This work was supported by the Horizon 2020 research and innovation programme under the Marie Skłodowska grant agreement No 837804 (DefTiMOFs, MSCA-IF-2018). I. A. L. thanks the European Union's Horizon 2020 research and innovation programme for receipt of the MSCA Individual Fellowship and The University of Valencia for research facilities. Connor JR Wells is acknowledged for proofreading this manusript.

References

1 A. Carné-Sánchez, I. Imaz, K. C. Stylianou and D. Maspoch, *Chem. – Eur. J.*, 2014, **20**, 5192–5201.
2 M. Safaei, M. M. Foroughi, N. Ebrahimpoor, S. Jahani, A. Omidi and M. Khatami, *TrAC, Trends Anal. Chem.*, 2019, **118**, 401–425.
3 P. Horcajada, C. Serre, M. Vallet-Regí, M. Sebban, F. Taulelle and G. Férey, *Angew. Chem., Int. Ed.*, 2006, **45**, 5974–5978.
4 M. Giménez-Marqués, T. Hidalgo, C. Serre and P. Horcajada, *Coord. Chem. Rev.*, 2016, **307**, 342–360.
5 P. Horcajada, R. Gref, T. Baati, P. K. Allan, G. Maurin, P. Couvreur, G. Férey, R. E. Morris and C. Serre, *Chem. Rev.*, 2012, **112**, 1232–1268.
6 I. A. Lázaro and R. S. Forgan, *Coord. Chem. Rev.*, 2019, **380**, 230–259.
7 J. W. M. Osterrieth and D. Fairen-Jimenez, *Biotechnol. J.*, 2021, **16**, 2000005.
8 R. J. Marshall and R. S. Forgan, *Eur. J. Inorg. Chem.*, 2016, 4310–4331.
9 H. Assi, G. Mouchaham, N. Steunou, T. Devic and C. Serre, *Chem. Soc. Rev.*, 2017, **46**, 3431–3452.
10 S. Yuan, J.-S. Qin, C. T. Lollar and H.-C. Zhou, *ACS Cent. Sci.*, 2018, **4**, 440–450.
11 X. Chen, X. Peng, L. Jiang, X. Yuan, H. Yu, H. Wang, J. Zhang and Q. Xia, *Chem. Eng. J.*, 2020, **395**, 125080.
12 J. Zhu, P.-Z. Li, W. Guo, Y. Zhao and R. Zou, *Coord. Chem. Rev.*, 2018, **359**, 80–101.
13 J.-L. Song, Z.-Q. Huang, J. Mao, W.-J. Chen, B. Wang, F.-W. Yang, S.-H. Liu, H.-J. Zhang, L.-P. Qiu and J.-H. Chen, *Chem. Eng. J.*, 2020, **396**, 125246.
14 Y. Xie, X. Liu, X. Ma, Y. Duan, Y. Yao and Q. Cai, *ACS Appl. Mater. Interfaces*, 2018, **10**, 13325–13332.
15 A. Rengaraj, P. Puthiaraj, N.-S. Heo, H. Lee, S. K. Hwang, S. Kwon, W.-S. Ahn and Y.-S. Huh, *Colloids Surf., B*, 2017, **160**, 1–10.
16 G. Lan, K. Ni, S. S. Veroneau, X. Feng, G. T. Nash, T. Luo, Z. Xu and W. Lin, *J. Am. Chem. Soc.*, 2019, **141**, 4204–4208.
17 J. Castells-Gil, N. M. Padial, N. Almora-Barrios, J. Albero, A. R. Ruiz-Salvador, J. González-Platas, H. García and C. Martí-Gastaldo, *Angew. Chem., Int. Ed.*, 2018, **57**, 8453–8457.
18 N. M. Padial, B. Lerma-Berlanga, N. Almora-Barrios, J. Castells-Gil, I. da Silva, M. de la Mata, S. I. Molina, J. Hernández-Saz, A. E. Platero-Prats, S. Tatay and C. Marti-Gastaldo, *J. Am. Chem. Soc.*, 2020, **142**, 6638–6648.
19 I. A. Lázaro, N. Almora-Barrios, S. Tatay and C. Martí-Gastaldo, *Chem. Sci.*, 2020, **12**, 2586–2593.
20 I. A. Lázaro, S. A. Lázaro and R. S. Forgan, *Chem. Commun.*, 2018, **54**, 2792–2795.
21 I. A. Lázaro, S. Haddad, J. M. Rodrigo-Muñoz, C. Orellana-Tavra, V. del Pozo, D. Fairen-Jimenez and R. S. Forgan, *ACS Appl. Mater. Interfaces*, 2018, **10**, 5255–5268.
22 I. A. Lázaro, C. J. R. Wells and R. S. Forgan, *Angew. Chem., Int. Ed.*, 2020, **59**, 5211–5217.

Open Access Article. Published on 16 July 2021. Downloaded on 4/8/2026 9:22:24 PM.
This article is licensed under a Creative Commons Attribution-NonCommercial 3.0 Unported Licence.

23 M. A. Dobrovolskaia and S. E. McNeil, *Nat. Nanotechnol.*, 2007, **2**, 469–478.
24 I. A. Lázaro, *Eur. J. Inorg. Chem.*, 2020, 4284–4294.
25 M. Taddei, K. C. Dümbgen, J. A. van Bokhoven and M. Ranocchiari, *Chem. Commun.*, 2016, **52**, 6411–6414.
26 C. Orellana-Tavra, R. J. Marshall, E. F. Baxter, I. A. Lázaro, A. Tao, A. K. Cheetham, R. S. Forgan and D. Fairen-Jimenez, *J. Mater. Chem. B*, 2016, **4**, 7697–7707.
27 E. Bellido, T. Hidalgo, M. V. Lozano, M. Guillevic, R. Simón-Vázquez, M. J. Santander-Ortega, Á. González-Fernández, C. Serre, M. J. Alonso and P. Horcajada, *Adv. Healthcare Mater.*, 2015, **4**, 1246–1257.
28 K. M. L. Taylor-Pashow, J. D. Rocca, Z. Xie, S. Tran and W. Lin, *J. Am. Chem. Soc.*, 2009, **131**, 14261–14263.
29 I. A. Lázaro, S. Haddad, J. M. Rodrigo-Muñoz, R. J. Marshall, B. Sastre, V. del Pozo, D. Fairen-Jimenez and R. S. Forgan, *ACS Appl. Mater. Interfaces*, 2018, **10**, 31146–31157.
30 P. Horcajada, T. Chalati, C. Serre, B. Gillet, C. Sebrie, T. Baati, J. F. Eubank, D. Heurtaux, P. Clayette, C. Kreuz, J.-S. Chang, Y. K. Hwang, V. Marsaud, P.-N. Bories, L. Cynober, S. Gil, G. Férey, P. Couvreur and R. Gref, *Nat. Mater.*, 2010, **9**, 172–178.
31 B. Maherani, E. Arab-Tehrany, A. Kheirolomoom, D. Geny and M. Linder, *Biochimie*, 2013, **95**, 2018–2033.
32 C. Orellana-Tavra, S. Haddad, R. J. Marshall, I. A. Lázaro, G. Boix, I. Imaz, D. Maspoch, R. S. Forgan and D. Fairen-Jimenez, *ACS Appl. Mater. Interfaces*, 2017, **9**, 35516–35525.
33 T.-G. Iversen, T. Skotland and K. Sandvig, *Nano Today*, 2011, **6**, 176–185.
34 A. D. Vos, K. Hendrickx, P. V. D. Voort, V. V. Speybroeck and K. Lejaeghere, *Chem. Mater.*, 2017, **29**, 3006–3019.

 This journal is © The Royal Society of Chemistry 2021